Particle emission rates during electrostatic spray deposition of TiO2 nanoparticle-based photoactive coating

Koivisto, Antti J.; Jensen, Alexander C. Ø.; Kling, Kirsten I.; Kling, Jens; Budtz, Hans Christian; Koponen, Ismo K.; Tuinman, Ilse; Hussein, Tareq; Jensen, Keld A.; Nørgaard, Asger Wisti

Total number of authors:
11

Published in:
Journal of Hazardous Materials

Link to article, DOI:
10.1016/j.jhazmat.2017.07.045

Publication date:
2017

Document Version
Publisher's PDF, also known as Version of record

Journal of Hazardous Materials 341 (2018) 218–227

Contents lists available at ScienceDirect

Journal of Hazardous Materials

journal homepage: www.elsevier.com/locate/jhazmat

Particle emission rates during electrostatic spray deposition of TiO_2 nanoparticle-based photoactive coating

Antti J. Koivisto[a,*], Alexander C.Ø. Jensen[a], Kirsten I. Kling[a], Jens Kling[b], Hans Christian Budtz[a], Ismo K. Koponen[a], Ilse Tuinman[c], Tareq Hussein[d], Keld A Jensen[a], Asger Nørgaard[a], Marcus Levin[a,e]

[a] National Research Centre for the Working Environment, Lersø Parkallé 105, Copenhagen, DK-2100, Denmark
[b] Center for Electron Nanoscopy, Technical University of Denmark, Fysikvej 307, DK-2800 Kgs., Lyngby, Denmark
[c] TNO, CBRN Protection, Lange Kleiweg 137, 2288 GJ, Rijswijk, Netherlands
[d] The University of Jordan, Faculty of Science, Department of Physics, Amman, JO-11942 Jordan
[e] ACT. Global, Kajakvej 2, 2770, Kastrup, Denmark

HIGHLIGHTS

- Electrostatic spray deposition (ESD) particle emissions are not well characterized.
- Emission rates in s^{-1} and $\mu g\ s^{-1}$ was defined for ESD of a photoactive nanocoating.
- Particle deposition rates and morphologies of deposited particle were determined.
- Emission rates and particle properties are required in exposure modellings.
- Recommendations for ESD process exposure modellings is given.

GRAPHICAL ABSTRACT

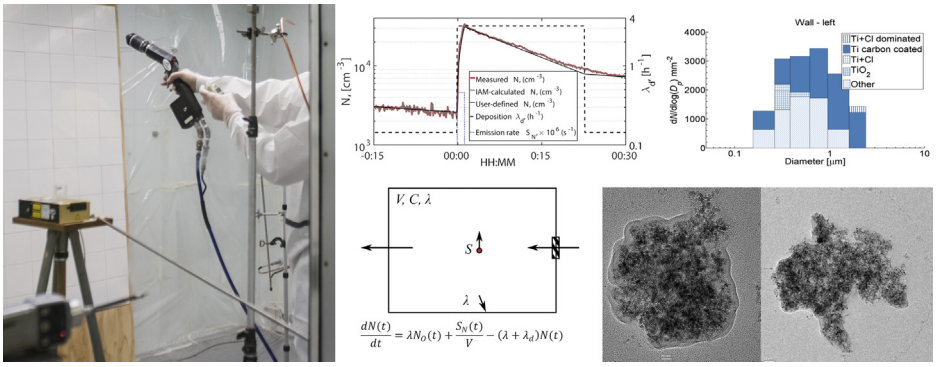

ARTICLE INFO

Article history:
Received 9 March 2017
Received in revised form 18 July 2017
Accepted 20 July 2017
Available online 29 July 2017

Keywords:
Electrostatic spray deposition
Indoor aerosol modeling
Emission rate
Deposition rate
Exposure modelling

ABSTRACT

Here, we studied the particle release rate during Electrostatic spray deposition of anatase-(TiO_2)-based photoactive coating onto tiles and wallpaper using a commercially available electrostatic spray device. Spraying was performed in a 20.3 m^3 test chamber while measuring concentrations of 5.6 nm to 31 µm-size particles and volatile organic compounds (VOC), as well as particle deposition onto room surfaces and on the spray gun user hand. The particle emission and deposition rates were quantified using aerosol mass balance modelling. The geometric mean particle number emission rate was $1.9 \times 10^{10}\ s^{-1}$ and the mean mass emission rate was 381 $\mu g\ s^{-1}$. The respirable mass emission-rate was 65% lower than observed for the entire measured size-range. The mass emission rates were linearly scalable (±ca. 20%) to the process duration. The particle deposition rates were up to 15 h^{-1} for <1 µm-size and the deposited particles consisted of mainly TiO_2, TiO_2 mixed with Cl and/or Ag, TiO_2 particles coated with carbon, and Ag particles with size ranging from 60 nm to ca. 5 µm. As expected, no significant VOC emissions were observed as a result of spraying. Finally, we provide recommendations for exposure model parameterization.

* Corresponding author.
E-mail addresses: jok@nfa.dk, jok@nrcwe.dk (A.J. Koivisto).

http://dx.doi.org/10.1016/j.jhazmat.2017.07.045

1. Introduction

Nanocoatings are highly transparent layers of polymers, metals or ceramics, which are typically below 100 nm, that can offer protection from ice formation, pollutants, UV-light, fire, heat, bacteria, marine life, wear and corrosion [1–4]. The superior properties of nanocoatings and lower material requirements are expected to motivate their application considerably in coming years. Moreover, the globally stringent volatile organic compound emission regulations are expected to also indirectly lead to an increase of the global nanocoating market volume to over 1200 kilo tons and an 8 billion US dollars revenue by 2020 [5]. In Japan, it was estimated that more than 50,000 m^2 of photoactive TiO_2 coating were already used in 2007 [6].

Photocatalytic materials have been known for many decades to remove various air pollutants under UV-light illumination [7]. Especially the development of TiO_2 based photoactive materials has enabled photocatalytic reaction under visible light, which increases the efficiency of photocatalytic oxidation and also enables the use of photocatalytic applications in indoor environments [8]. Photocatalytic oxidation of TiO_2 generates free radicals which induces redox reactions of absorbed substances and changes surface properties to super-hydrophilic, which then can be cleaned efficiently with water [6,9]. These two properties make photocatalytic surfaces self-cleaning, antimicrobial, and oxidative for organic pollutants [1,2,6,8–15].

Antimicrobial surface properties are desired in health care facilities and public domains to reduce the risk of infection disease outbreaks [16,17]. Pulliam [18] demonstrated how photocatalytic TiO_2 coatings reduced overall infection rates by 30% in a health care facility. Photocatalytic coatings have also been shown to reduce common urban air pollutants, such as e.g. nitrogen oxides, sulfur oxides, volatile organic compounds (VOCs), ammonia, carbon monoxide and hydrogen sulfide, in both indoor [19–21] and outdoor environments [12,14,15,22–24]. However, the formation and health effect of potential by-products formed from photocatalytic oxidation reactions are not fully understood [24].

Spraying is a common technique to apply nanocoatings onto surfaces. Consumer products are usually applied using propellant and pump sprays [25], while spray guns or electrostatic spray deposition (ESD) systems are mainly used in industrial applications [26–30]. The transfer efficiency, i.e. the fraction of precursor sprayed that coats the surface, depends on the spray gun settings and spraying conditions [31]. Transfer efficiencies of the ESD systems are expected to be higher than propellant and pump sprays or air spray guns because the sprayed particles are charged which deposition onto the surfaces is increased due to image charge force as compared to that of neutral particles. In agricultural ESD applications the spray mass-transfer to the target is generally verified to be 2–8 times higher than using conventional spraying techniques [27]. Also, the deposition of charged particles can be controlled by electric fields due to Coulomb force [32].

Here we studied particle emission rates and deposition of the particles during ESD coating using a commercially available electrostatic spray device. The ESD device was used to apply a suspended anatase-(TiO_2)-based photoactive coating onto tiles and wallpaper. The particle content in the non-sprayed bulk liquid (reference samples) was characterized. We measured size resolved airborne particle concentrations using real time aerosol instruments. From the measured particle concentrations we resolved particle emission rates (particles s^{-1} and $\mu g\ s^{-1}$) and particle deposition rates using indoor aerosol modelling (IAM). Deposited particles were collected passively on sampling substrates mounted on the operators' gloves, floor and walls, which were not directly sprayed. Size, morphology, and size-resolved chemical composition of deposited particles were defined as concentrations of particles mm^{-2}. The emission rates, deposition rates and properties of deposited particles can be used for personal and environmental exposure assessment.

2. Methods

2.1. Coating product

The product tested in this study is called CleanCoat® (ACT.Global, Kastrup, Denmark). The product consists of anatase-(TiO_2) particles (n.a. wt.%) and silver chloride (n.a. wt.%) in a hydrous medium with 2 wt.% 2-propanol and acidified by HNO_3 to pH 0.78. After application, the coating facilitates photocatalytic oxidation of VOCs and deposited particles. The product is classified as a biocide. In this study was used a CleanCoat® product where anatase-(TiO_2) concentration was 0.2 wt.%.

2.2. Product analysis

After shaking the bottle by hand following the instructions of the manufacturer, samples of the liquid product were taken and transferred to analysis. 10 mL were filled in standard 40mm-liquid-sample-cups with polypropylene foil for XRF-analysis. The inorganic content in the bulk liquid was measured with a standardless detection method (QuantExpress, SpectraPlus V.2, Bruker) in a WDXRF Tiger S8 4 kV instrument (Bruker AXS GmbH, Karlsruhe, Germany). Results are given in elemental wt.% normalized to 100%, adding water as a matrix component and a fixed value of 2% propanol to the calculation.

Some was dropped on Silicon wafer pieces of 1 cm^2 and on Cu-TEM grids with a C-membrane. The particle size, morphology and chemical composition were measured in a scanning electron microscope (Helios EBS3, FEI, Eindhoven, The Netherlands) with an energy dispersive X-ray detector (EDAX SD Apollo 10 Pegasus System) and software (EDAX Genesis, EDAX, Mahwah, NJ, USA). Primary particle size and crystal structure were determined in a transmission electron microscope (Titan ETEM, FEI, Eindhoven, The Netherlands).

2.3. Spray application and test room

The CleanCoat® product was sprayed using an electrostatic spray system (model SC-ET, Electrostatic Spraying Systems, Watkinsville, GA, USA). The gravimetric liquid mass flow rate was $0.9 \pm 0.02\ g\ s^{-1}$ and the atomizer flow (compressed air) was $1.9\ L\ s^{-1}$. The nozzle voltage, charging the particle after atomizing the precursor, was 1.2–1.3 kV.

Fig. 1a shows the test room (20.3 m^3) where the experiments were carried out at $23 \pm 0.5\ ^\circ C$ and $50 \pm 3\%$ relative humidity at an air exchange rate of $0.5 \pm 0.05\ h^{-1}$. The ventilation air supply was filtered through a F7 class (according to EN 779:2012 [33]) particle and molecular filter (City-Flo XL, Camfill, Aarhus, Denmark) and taken from the roof of the building (Lersø Parkallé 105, Copenhagen, Denmark). The test room ventilation air was supplied and exhausted from ventilation dispensers located at half of the room height (Fig. 1a). The pressure difference of the room compared to the surrounding environment was 0 ± 1 Pa.

The spraying was applied continuously for ca. 15 and 150 s to an upright 2 m^2 electrically ungrounded surface of either tiles or wallpaper. According to the manufacturer, the continuous coating rate is ca. 23 $m^2\ min^{-1}$. The spraying of the 2 m^2 surface lasted ca. 5 s after which spraying was continued on already sprayed surface. Spraying was started from the up-left corner and applied using

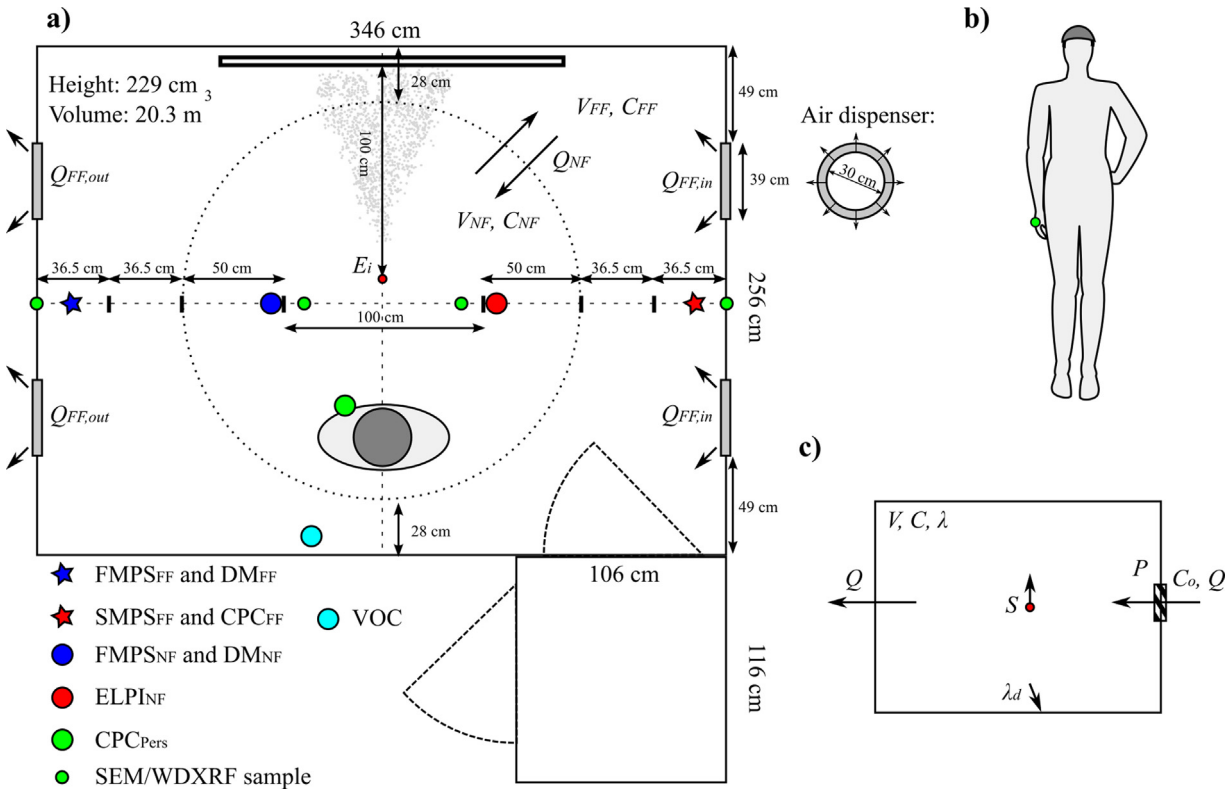

Fig. 1. Sketch of: a) the spray test chamber with sampling points, worker position, and position of the spray gun during use, b) position of personal passive particle deposition sampling substrates, and c) the conceptual mass-balance model for airborne particles.

S-shaped horizontal stroke. At the end of the spraying process, the spray gun was switched off and operator left the room within 60 s.

2.4. Collection and analysis of deposited particles

Silicon wafer pieces of 1 and 4 cm^2 and Nuclepore filters (WhatmanTM, d 37 mm) were mounted on the floor, walls and surfaces of other equipment at height of 120 cm (Fig. 1a) to quantify the loss and composition of particles to room surfaces in Near Field (NF) and Far Field (FF). Sampling of personal deposited spray particles were also made using the sampling substrates mounted on the operator's hand holding the spray gun (Fig. 1b). All sampling substrates were mounted immediately before each experiment and only exposed during the time of the experiments. After sampling was completed they were packed, sealed and stored in small containers at ca. 23 °C and between 35 and 52% relative humidity. The particle size, morphology and size-resolved chemical composition were derived from secondary electron (SE) images of silicon wafers measured in a scanning electron microscope (SEM; Helios EBS3, FEI, Eindhoven, The Netherlands) with an energy dispersive X-ray detector (EDAX SD Apollo 10 Pegasus System) and software allowing for automated single particle analysis (EDAX Genesis Particles, EDAX, Mahwah, NJ, USA). Nuclepore filters were analyzed by means of wavelength dispersive x-ray fluorescence analysis (WDXRF). A method measuring the amount of Ag collected on the filters was setup in a WDXRF Tiger S8 (Bruker, Karlsruhe, Germany). A mask of 34 mm was applied and the measured area was calculated to 907 mm^2.

2.5. VOC sampling and analysis

VOCs were sampled through a 10 mm stainless steel sampling manifold placed at a height of 100 cm (Fig. 1a). Prior to spraying the product, a background sample was collected from the chamber. Samples were taken in duplicates at 10–60 min intervals, starting at the first sampling event 1–3 min after application of the spray. The time of sampling is given as the midpoint between start and end of each sampling period. The VOCs were sampled on Tenax TA adsorbent tubes (60–80 mesh, 200 mg) at a sampling time of 10 min at 100 mL min^{-1} using calibrated pumps (Gillian Gilair 5, Sensidyne, US). The Tenax TA tubes were analyzed on a Perkin Elmer Turbo Matrix 350 thermal desorber coupled to a Bruker SCION TQ GC–MS system (Bruker Daltonics, Bremen, DE). Tube desorption was carried out at 275 °C for 20 min and the low and high temperatures of the cryo-trap were −20 °C and 280 °C, respectively. The gas chromatography column was a 30 m × 0.25 mm with 0.25 μm film thickness; VF-5MS (Agilent Technologies, Santa Clara, US). The oven program was: 50 °C for 4 min following thermal increase at rate of 4 °C min^{-1} to 120 °C and then thermal increase at rate of 50 °C min^{-1} to 250 °C where temperature was hold for 2 min. Helium was used as carrier gas at an inlet pressure of 0.97 bar (1.5 mL min^{-1}). The mass spectrometer was operated in Scan mode (m z^{-1} 35–500) using electron ionization. Valves, transfer lines and ion source were kept at 270 °C. Six-point calibration was applied ($r^2 > 0.99$) using toluene in methanol. Measured VOCs are thus reported in toluene equivalents as the mean of duplicates corrected for the contents in the background air and rounded to nearest integer.

2.6. Real-time particle measurements

The particle concentrations and size-distributions were measured from 50 cm (NF) and 155 cm (FF) from the spray gun at height of 115 cm (half of the room height; Fig. 1a). All instruments, except the dust monitors, were placed outside of the room. The sampling lines were electrically conductive and diffusion losses were corrected according to Cheng [34].

Both the NF and FF particle size-distributions were measured from 5.6 nm to 560 nm in 1 s intervals with two Fast Mobility Particle Sizers ($FMPS_{NF}$ and $FMPS_{FF}$ TSI model 3091, TSI Inc., Shoreview, MN, USA) and from 250 nm to 31 μm in 6 s intervals with two Dust Monitors (DM_{NF} and DM_{FF}, Grimm Model 1.109, Grimm Aerosoltechnik, Ainring, Germany). The $FMPS_{NF}$ and DM_{NF} particle number concentrations, N (cm^{-3}), were combined as one $dN/dLog(D_{pg})$ particle number size-distribution where D_{pg} (m) is the geometric mean diameter [35]. Here, the $FMPS_{NF}$ concentrations was averaged to 6 s and size channels with $D_{pg} > 254.8$ nm were removed and was cut so that the upper boundary limit was the same as the DM_{NF} smallest size bin lower boundary limit. Then, D_{pg} and $dLog(D_{pg})$ values were calculated for the cut size-bin. The combined particle size-distribution, named as $FMPS_{NF} + DM_{NF}$, was based on the mobility size concentrations from 5.6 to 252.8 nm and optical size concentrations from 252.8 nm to 31 μm. Here, we assumed that mobility and optical particle diameters are the same.

The NF particle size-distributions were also measured from 6 nm to 10 μm in 1 s intervals with an Electrical Low Pressure Impactor ($ELPI_{NF}$, Dekati model ELPI+, Dekati Ltd., Tampere, Finland).

The FF particle size-distributions measured from 8.8 to 310.6 nm in 60 s intervals with a Scanning Mobility Particle Sizer ($SMPS_{FF}$, TSI Inc., Shoreview, MN, USA), which consisted of a classifier (TSI Classifier model 3082), a soft X-ray neutralizer (TSI model 3088), a differential mobility analyzer (DMA, TSI model 3081 sheath air flow 8.0 L min^{-1}), and a condensation particle counter (CPC, TSI model 3010, Qs = 1.2 L min^{-1}). The SMPS scan time was 47 s with a 13 s retrace time. An additional CPC (CPC_{FF}, TSI model 3007) measured the particle number-concentrations from the SMPS sampling line at 1 s resolution.

Breathing zone particle number-concentrations were measured using a Grimm CPC (CPC_{Pers}, Grimm model 5.400, Grimm Aerosoltechnik, Ainring, Germany).

2.7. Dynamics of aerosol particles

Dynamics of airborne particle number concentrations were described by using a single compartment mass-balance model (Fig. 1c) [36]. Here, it was applied to calculate the sub-micrometer ($D_p < 1$ μm) and micrometer ($D_p \geq 1$ μm) particle concentration change, dN/dt (s^{-1} m^{-3}), in the room as:

$$\frac{dN(t)}{dt} = \lambda N_0(t) + \frac{S_N(t)}{V} - (\lambda + \lambda_d)N(t) \quad (1)$$

where N (cm^{-3}) is the particle number concentration, t (s) is the time, λ (s^{-1}) is the ventilation rate, N_O (cm^{-3}) is the incoming air particle number concentration, S_N (s^{-1}) is the particle number emission rate, V (m^3) is the volume of the test room, and λ_d (s^{-1}) is the deposition rate of the particles. The model assumes that particle concentrations are fully mixed all the time and coagulation is negligible.

Particles are lost from the room air by general ventilation and deposition onto the surfaces. The particle removal rate by ventilation equals to the ventilation rate of 0.5 h^{-1} when concentrations are assumed fully mixed. Particle deposition to ceiling ($\lambda_{d,ceiling}$), walls ($\lambda_{d,walls}$), and floor ($\lambda_{d,floor}$) were calculated from measured particle number concentrations using a deposition model [37] for particles in charge equilibrium. The estimate for electrostatic deposition ($\lambda_{d,es}$) was defined from the mathematical difference between measured and modelled concentrations when coagulation was ignored [38].

2.8. Emission rates

The particle number S_N (s^{-1}) and mass S_m (μg s^{-1}) emission rates were estimated from the measured particle number N (cm^{-3}) and mass m (μg m^{-3}) concentrations using the mass balance Eq. (1), and spray duration, t_{ESD} (s). Two different techniques were used to predict emission rates: 1) the mass balance Eq. (1) was used to predict how many particles need to be generated or removed in order to obtain the measured level [37] (IAM calculated) which was then further averaged (user-defined); and 2) emission rates were calculated from the amount of airborne particles and spray duration as:

$$S_C = \frac{\bar{C} \cdot V}{t_{ESD}} \quad (2)$$

where $\bar{C}$ is the mean concentration of particles in number (m^{-3}) or mass (μg m^{-3}) during the spraying process and V is the room volume (m^3). Here is assumed that initial particle concentration is low compared to concentration during spraying, particle removal processes by ventilation and deposition are negligible, and concentrations are fully mixed in the room.

3. Results and discussion

3.1. Product analysis

The WDXRF analyses of the liquid product (reference material) confirmed the composition given by the supplier within a range of a few ppm. The geometric mean particle diameter of primary TiO_2 particles observed in agglomerates measured from TEM-images of the reference material was 5.5 nm with a standard deviation of 1.5 nm (n = 21). Results from chemical and structural analyses using SEM/EDS and TEM suggest that Ag and TiO_2 are present as two separate phases. Ag primary particles were around 10–15 nm in diameter. The dispersed particles build a film composed of primary grains all over the analyzed substrates upon drying. The Ag particles show a higher contrast in TEM (Fig. 2a). The EDS spectrum (not shown) of the particle in Fig. 2a shows Ag and no Cl signal, which indicates that the particles were deposited as Ag, not AgCl. Diffraction analysis of comparable particles also indicates Ag structure. But the presence of individual Cl containing Ag particles cannot be excluded.

Re-dispersed particles on the Si wafer for SEM were investigated on the micron scale. It must be noted that particles baked together and formed a crust of particle suspended over the Si wafer. The crust was composed of TiO2. In or on the bulky crust, larger particles with a higher back-scattered electron contrast (brighter) were observed, those particles contained Ag.

Due to the high abundance of TiO_2, it was not possible to prove the purity of Ag-particles or determine whether any other elements were associated with the Ag. Cl was not detected in the particles investigated, because the preparation was focused on the hard particulate content of the product. Thus it must be noted that the morphology and dispersion of particles collected from the liquid product was different from the appearance of particles on the passive-deposition samples, most likely due to lower concentration and better dispersion of sprayed particles. However, the primary particle size of TiO_2 in agglomerates was confirmed also for the passive deposition samples by high resolution SEM images.

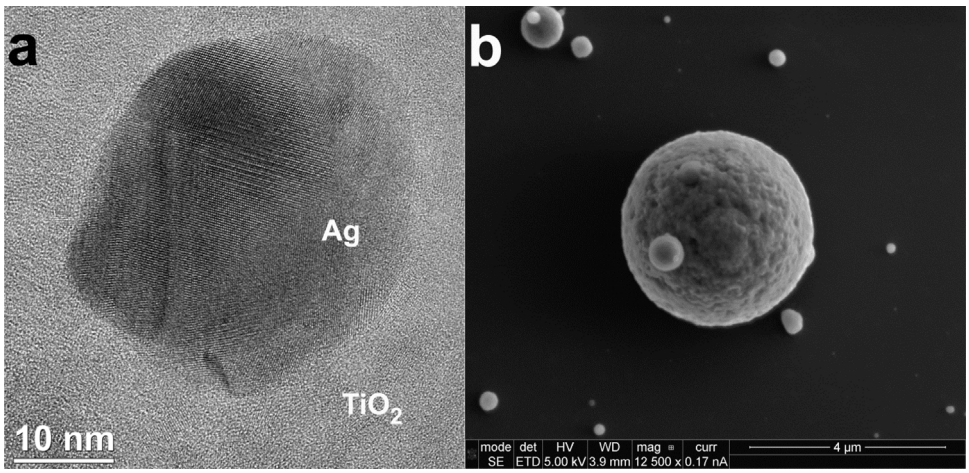

Fig. 2. a) High-resolution TEM image of suspended reference material of and Ag nanoparticle (verified by EDS), b) SEM secondary electron image of deposited material on a silicon wafer showing spheroidal agglomerates consisting of TiO_2 and Ag nanoparticles.

3.2. Estimations of density from EM images and chemical analysis

Based on primary particle size and agglomerate size, the assumption was made that they are homogeneously packed close to 74% (FCC packing) and the space between the primary particles is filled with lighter material which was assumed to be hydrochloric acid (density 1.49 g cm^{-3}). With the density of TiO_2 4.23 g cm^{-3} the round shaped agglomerate density is 3.51 g cm^{-3}. Fig. 2b shows an overview image of a typical round shaped, densly packed agglomerate.

During ESD process, these agglomerates are suspended in atomized droplets. The droplet suspension contained nitric acid which prevent the droplet evaporation under typical indoor atmosphere. The droplets were assumed to be spherical and consist mainly of water which density was 1 g cm^{-3}.

3.3. Total VOC concentrations

There was no significant difference in the total VOC concentration between the background sample and the samples after spraying (Fig. S1). The total VOC concentrations were for the background measurements at maximum of 48 µg m^{-3} and 7, 25, and 145 min after spraying 31, 56, and 7 µg m^{-3}, respectively. The lower total VOC concentrations measured after spraying are due to uncertainties in the measurements. The VOC background from the Tenax adsorbent and the cold trap was high compared to the concentration of sampled VOCs. The results are as expected due to the product formulation which contains only isopropanol as VOC according to the table of contents. Isopropanol will not be measured by this method due to poor adsorption on Tenax adsorbent.

3.4. Particle concentrations

The spray durations on the tiles were 15 and 150 s (T15 and T150, respectively) and 18 and 150 s on wallpaper (W18 and W150, respectively) which corresponds to ejection of 13.5, 135, 16.2 and 135 g of CleanCoat® suspension, respectively. The real-time NF and FF measurements revealed that the concentrations were well-mixed in the room within 10 s (Fig. S2). The particle number size-distributions measured by the $FMPS_{NF}$+DM_{NF} covered particles ranging in diameter from below the FMPS detection limit of 5.6 nm to ca. 30 µm (Figs. 3 and S3).

The particle number size-distribution was converted to particle mass size-distribution (Figs. S3b and S5) using the droplet density of 1 g cm^{-3}. Calculated mass concentrations varied from 30 to 460 µg m^{-3} for particles < 1 µm and from 180 to 2890 µg m^{-3} for particles ≥ 1 µm, when averaged from start of spraying to 60 s after end of spraying (Table S2). This corresponds to a geometric mean transfer efficiency of 99.96% (GSD = 1.0001). In a spraying booth, typical transfer efficiencies for conventional air spraying guns have been determined to vary from ca. 70–92% [39]. However, the transfer efficiency measured by Tan and Flynn [39] is the ratio of the dry paint mass applied to the target and mass of the solid components which may not be comparable with the transfer efficiency calculated in this study.

3.5. Particle deposition and emission rates

Airborne particles mass balance was solved separately for submicrometer and micrometer particles except in T15, where the micrometer particle concentrations were too low. The measured and modelled number concentrations as well as deposition and emission rates are shown in Fig. 4 for W18 and W150 and in Fig. S4 for T15 and T150. The total calculated particle deposition rates for the aerosol in a charge equilibrium ($\lambda_{d,ceiling}$+$\lambda_{d,walls}$+$\lambda_{d,floor}$) was up to 0.07 h^{-1} for particles <1 µm and up to 0.24 h^{-1} for particles ≥ 1 µm. The electrostatic deposition ($\lambda_{d,es}$) rate was up to 15 h^{-1} for particles <1 µm and up to 1.05 h^{-1} for particles ≥ 1 µm (Table S1).

Because the user-defined emission rates were not constant an average S_N was calculated by normalizing the total number of emitted particles with the spraying time (Table 1) which geometric mean was 3.6×10^{10} s^{-1} (GSD = 1.8). According to Eq. (2) the geometric mean S_N was 1.9×10^{10} s^{-1} (GSD=3.9). In principle, the transfer efficiency should be independent of spraying time and spraying target when the orientation is the same. Thus, the emission rates should be similar in different experiments. However, here the tiles and wallpaper were not grounded and the spraying was performed on already sprayed surfaces. The particles may charge the surface and reduce the deposition efficiency of particles with the same charge. This may explain higher emission rates in 150 s spray experiments than in 15 and 18 s spray experiments (Table 1).

According to Eq. (2) the geometric mean S_m was 381 µg s^{-1} (GSD = 1.3) and there was good repeatability regardless of the spray

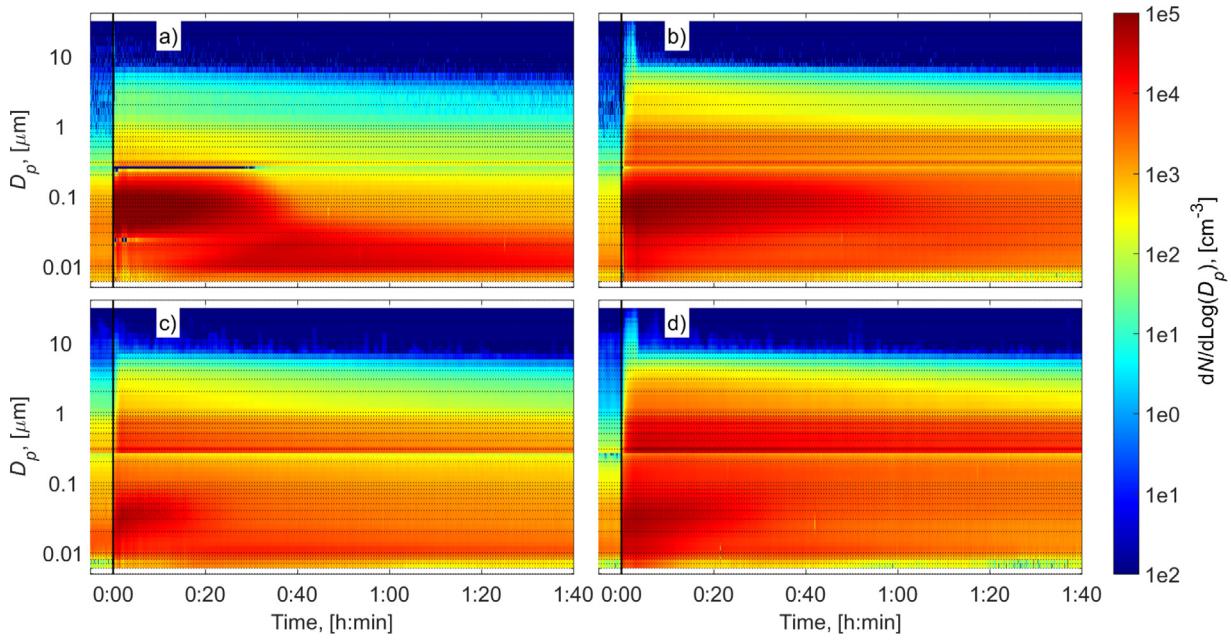

Fig. 3. Particle number size-distributions measured by the $FMPS_{NF}$+DM_{NF} during spraying on tiles for a) 15 s and b) 150 s; and on wallpaper for c) 18 s and d) 150 s. The vertical black lines show the start time of the spraying.

time or target material (Table S3). According to the simplified respirable fraction penetration efficiency [40], the geometric mean respirable mass emission rate, $S_{m,respirable}$, was 171 μg s^{-1}. The size-resolved S_N, S_m, and $S_{m,respirable}$ calculated using Eq. (2) are given in the Supplementary data. The emission rates will be implemented into an emission library [41], which is used for personal and environmental exposure modelling.

For a comparison, the mass emission rates were calculated using the particle number concentration log-normal distribution D_{pg} and GSD parameters and the user-defined emission rate S_N shown in (Table S3). This resulted in a geometric mean total mass emission rate of 212 μg s^{-1} (GSD = 3.4) when experiment T15 was not taken into account. The average mass concentrations calculated from log-normal distribution parameters varied from 0.2 to 10 times the measured mass concentration (Table S3). In this case, the conversion using log-normal distribution parameters underestimates the mass concentrations. A larger difference in emission rates calculated by these two methods was expected, because the measured particle number size-distributions for $D_p < 1$ μm and for $D_p \geq 1$ μm were not log-normally distributed. However, room mass concentrations calculated using mass emission rates defined according to Eq. (2) gave nearly the same results, as derived from Eq. (1). It must be noted that there is always high uncertainty in particle number size-distribution conversion to particle mass size-distribution because the particle diameter often depends on the detection technique and the number count error propagates in mass conversion to power 3.

Mass concentration ratio for T150 and T15 experiments was 11.6 when 10 was expected and for W150 and W18 experiments was 7.7 when 8.3 was expected according to spray durations. Thus, the mass-emissions scaled linearly (±ca. 20%) between the short and long spray durations.

3.6. Composition of deposited particles

According to the EM and EDS analyses, the deposited particles consisted mainly of TiO_2, TiO_2 containing Cl or Ag, TiO_2 coated with carbon and to minor extent other particles, Ag, and AgCl particles (Fig. 5). The deposited non-evaporated particles were predominantly present in the size range from 200 nm to <5 μm in geometric diameter in the wall and floor samples; and from 60 nm to 2 μm in the person hand sample. The NF right-side sample concentrations were clearly higher than the NF left-side sample concentration, which is anticipated because the spray gun was held in the right hand. The hand was exposed to the room concentrations during spraying for 150 s and ca. 60 s before the operator left the room. Particle deposition to the hand was calculated using the total deposition rate $\lambda_d = 0.0517$ h^{-1} for the first 42 s and then 1.25 h^{-1} (Table

Table 1
Log-normal parameters (N, D_{pg}, and GSD) calculated for average particle number concentrations measured from start of the spraying to 60 s after the end of the spraying and average user-defined emission rates for sub-micrometer particles and micrometer particles.

Experiment	Sub-micrometer particles ($D_p < 1$ μm)				Micrometer particles ($D_p \geq 1$ μm)			
	N, × 10^3 [cm^{-3}]	D_{pg}, [nm]	GSD	S_N, × 10^{10} [s^{-1}]	N, [cm^{-3}]	D_{pg}, [nm]	GSD	S_N, × 10^6 [s^{-1}]
T15	89.8	52.3	1.65	2.8 (4.4)[a]	17	1.81	1.6	n.a.[b]
T150	53.2	50.3	2.13	6.1 (3.9)	150	1.85	1.62	6.0 (2.6)
W18	22.1	29.0	2.47	1.8 (2.1)	69	1.61	1.44	40 (1.4)
W150	47.5	40.9	3.15	5.5 (3.1)	418	1.65	1.48	22 (2.8)

[a] Brackets shows the geometric standard deviation calculated from IAM-calculated emission rates when user-defined S > 0.
[b] n.a.: not available.

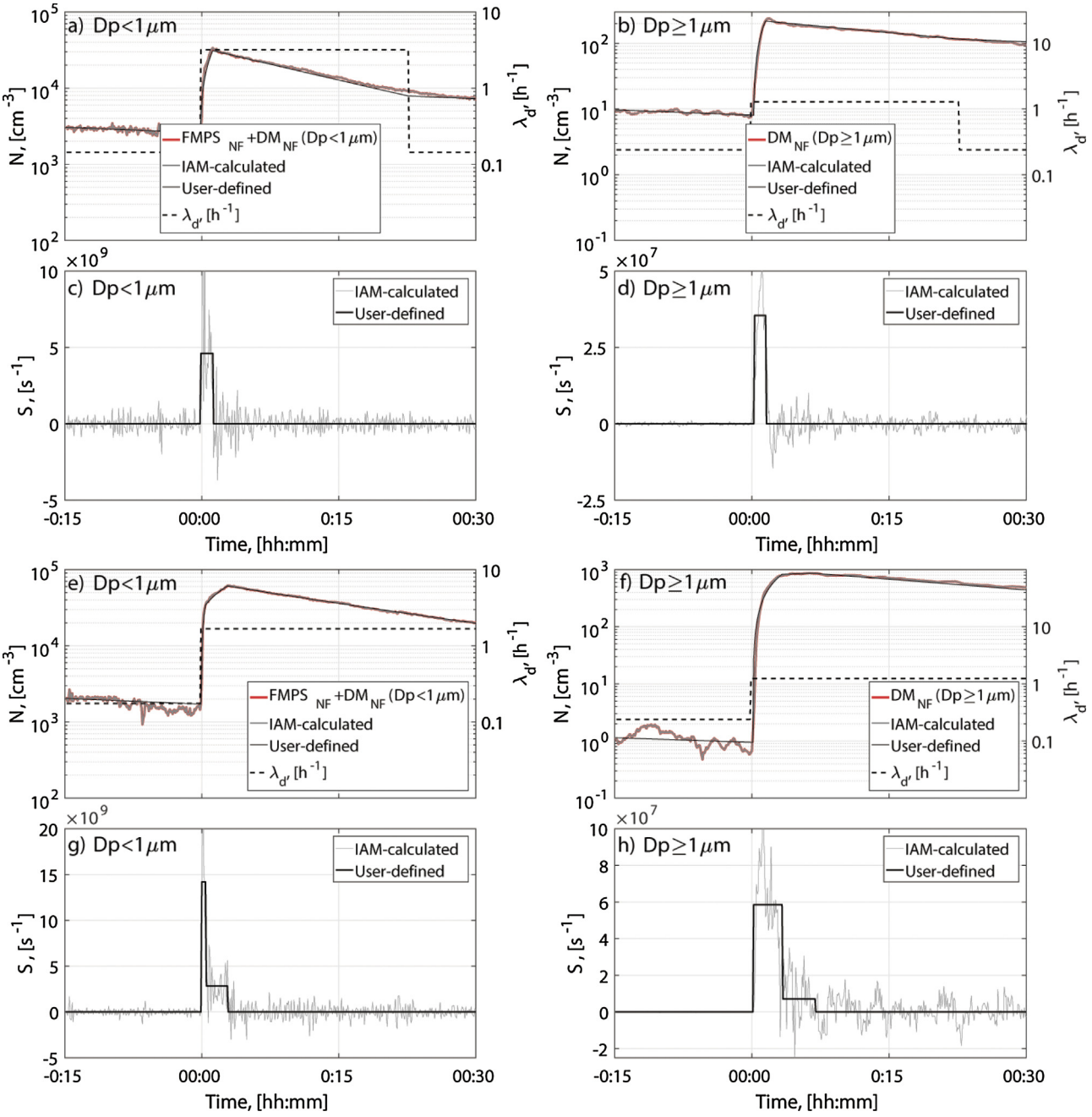

Fig. 4. Measured, IAM calculated, and user defined particle concentrations and deposition rates in the W18 experiment for a) sub-micrometer particles and b) micrometer particles as well as modelled and user defined emission rates for c) sub-micrometer particles and d) micrometer particles, respectively, and in the W150 experiment for e) sub-micrometer particles and f) micrometer particles as well as modelled and user defined emission rates for g) sub-micrometer particles and h) micrometer particles, respectively.

S1) and using average particle concentration of 53.3×10^3 cm^{-3} (Table 1). This results to ca. 1800 deposited particles mm^{-2} which is ca. 5 times less than detected by the EM (Fig. 5e). This might be due to the movement of the hand into the spray cloud during spray application and consequently increased deposition and impaction of particles on the substrate.

The results from the WDXRF analysis show similar average concentrations of around 50 ppm Ag on all filters based on three measurements. The detection limit of the method is slightly below 50 ppm and the uncertainty thus is very high. Some measurements were below detection limit and measured as 0 ppm. Those were included in the average. Thus, no significant difference was found between the different locations, so we assume that the particles were well mixed in the room before settling to the walls and the floor.

3.7. Recommendations for personal exposure modelling

Personal exposure models are often based on single compartment [42] or two compartment models (also known as NF/FF model; [43]). In worst case consumer exposure assessment the default room size is 20 m^3 and the room is not ventilated [44], which is close to our experimental setup conditions. It is expected that after ESD process, the operator leaves the room within up to

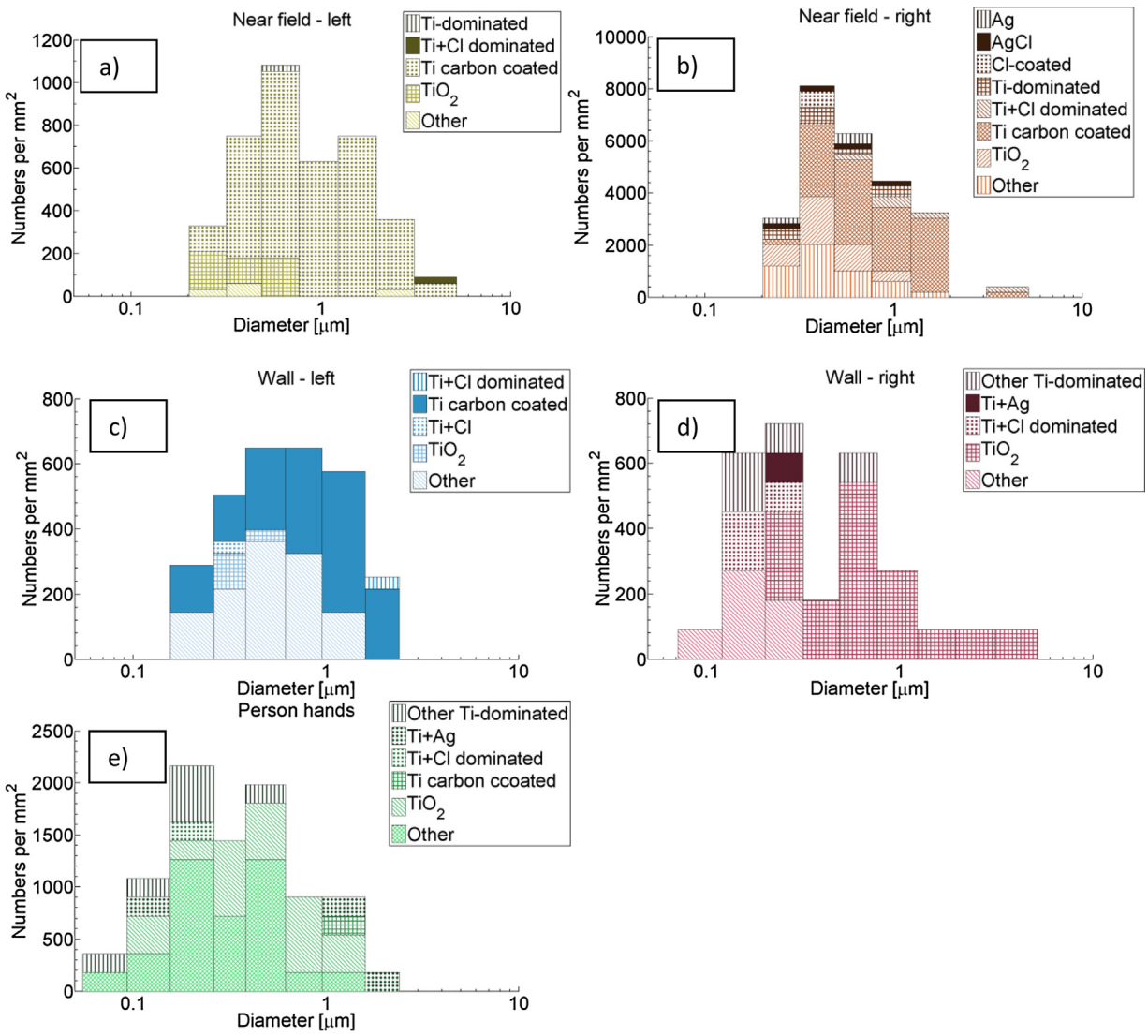

Fig. 5. Size-distributions of particles deposited onto passive samplers during T150 experiment as determined by semi-automated compositional particle analysis using EDS-SEM.

10 min. In our experiments, the average mass (number) concentration during coating of wallpaper for 750 s would be ca. 3200 μg m^3 (54×10^3 cm^{-3}) where 35% is in the respirable size-range. We measured increased particle deposition onto surfaces ranging from 0.75 to 3.12 h^{-1} for micrometer particles which means that the room concentration is halved in 55–13 min, respectively. The deposition of particles to the hand holding the spray gun can be estimated from average particle number exposure concentration and the deposition rate. In this case, the calculated amount of deposited particles would be ca. 8.0×10^3 mm^{-2} which may be underestimated by factor of 5 as compared to measured values by EM and EDS analysis.

A NF/FF model is recommended for exposure assessment in large rooms. In the NF/FF model a room is divided into NF volume (V_{NF}, m^3) that compromises the source and a worker breathing zone and the FF volume (V_{FF}, m^3) which compromise rest of the room (i.e. $V_{tot} = V_{NF} + V_{FF}$). The room is ventilated via FF (Q, m^3 s^{-1}) and there is a limited air flow between the NF and FF volumes (β, m^3 s^{-1}). It is assumed that: 1) all mass entering the model is created by a source in the NF volume, 2) concentrations are fully mixed at all the times in NF and FF volumes, 3) there are no other losses for the concentrations than the FF ventilation, and 4) there is no significant cross drafts [45].

Typically β varies from 0.05 to 0.5 m^3 s^{-1} in occupational settings [46] and usually V_{NF} is set to 8 m^3 [46–48]. Here, the spray gun air flow was 1.9 L s^{-1} which was sufficient to fully mix the air in a 20.3 m^3 room. Thus, we recommend that the V_{NF} should be at least 20.3 m^3 and the β should be high (e.g. from 0.2 to 0.5 m^3 s^{-1}). This is because the concentrations were fully mixed in the room air within 10 s. The size-resolved emission rates for each experiment are given in Supplementary data as particle number (s^{-1}) and mass (μg s^{-1}) units. The emissions may change if the spray gun design, suspension, spray technique, or target properties are changed.

4. Conclusion

Here we studied the aerosol emission characteristics for electrostatic spray deposition (ESD) of a photoactive nanocoating onto tiles and wallpaper. We determined size-resolved emission rates in number (S_N, s^{-1}) and mass (S_m, μg s^{-1}), release of volatile organic compounds (VOCs), deposition rates of emitted particles,

and described the particle morphologies and compositions in the product and deposited from the air to un-targeted surfaces and the spray gun operator hand.

The transfer efficiency of the ESD was 99.96% and the S_N was $1.9 \times 10^{10}\,s^{-1}$ and the S_m was $381\,\mu g\,s^{-1}$ where ca. 35% of the mass was respirable. The mass-based emission rates scaled linearly between the ca. 15 s to 150 s spray time with an accuracy of ca. 20%. Longer spray-time increased the S_N but S_m was similar regardless the spray time during these short-term application scenarios. This was likely caused by the spraying performed on already sprayed surfaces which were not grounded. During spraying, VOC-concentration was elevated from the background level less than $8\,\mu g\,m^{-3}$. The deposited particles consisted of mainly TiO_2, TiO_2 containing Cl or Ag, TiO_2 coated with carbon and other particles with sizes from ca. 60 nm to <5 μm depending on the sampler location (walls, floor, or operator hand). Finally, we gave recommentdations for the exposure model parameterization.

Acknowledgements

The research leading to these results has received funding from the European Union Seventh Framework Programme [FP7/2007-2013] underEC-GA No. 604305 'SUN' and Danish Innovation Fund project 5112-00004B. We thank ACT.Global for supplying the product used in the study, the spraying equipment and for conducting the spraying.

Appendix A. Supplementary data

Supplementary data associated with this article can be found, in the online version, at http://dx.doi.org/10.1016/j.jhazmat.2017.07.045.

References

[1] K. Hashimoto, H. Irie, A. Fujishima, TiO2 photocatalysis a historical overview and future prospects, Jpn. J. Appl. Phys. 44 (2005) 8269–8285.
[2] F. Pacheco-Torgal, S. Jalali, Nanotechnology advantages and drawbacks in the field of construction and building materials, Constr. Build. Mater. 25 (2011) 582–590.
[3] M.J. Hanus, A.T. Harris, Nanotechnology innovations for the construction industry, Prog. Mater. Sci. 58 (2013) 1056–1102.
[4] B.P. Jelle, A. Hynd, A. Gustavsen, D. Arasteh, H. Goudey, H. Hart, Fenestration of today and tomorrow: a state-of-the-art review and future research opportunities, Sol. Energ. Mat. Sol. Cells. 96 (2012) 1–28.
[5] Grand View Research, Nanocoatings Market Analysis By Product (Anti-Fingerprint, Anti-Microbial, Anti-Fouling & Easy-To-Clean, Self-Cleaning), By Application (Healthcare, Food, Packaging, Marine, Water Treatment, Electronics, Construction, Automotive, Energy) And Segment Forecasts To 2020. Grand View Research, Inc. October 2014. ISBN: 978-1-68038-247-1.
[6] J. Ângelo, L. Andrade, L.M. Madeira, A. Mendes, An overview of photocatalysis phenomena applied to NOx abatement, J. Environ. Manag. 129 (2013) 522–539.
[7] T. Ibusuki, K. Takeuchi, Removal of low concentration nitrogen oxides through photo assisted heterogeneous catalysis, J. Mol. Catal. 88 (1994) 93–102.
[8] J. Chen, F. Qiu, Q. Xu, S. Cao, H. Zhu, Recent progress in enhancing photocatalytic efficiency of TiO2-based materials, Appl. Catal. A Gen. 495 (2015) 131–140.
[9] J. Chen, C.-S. Poon, Photocatalytic construction and building materials: from fundamentals to applications, Build. Environ. 44 (2009) 1899–1906.
[10] N.S. Allen, M. Edge, J. Verran, J. Stratton, J. Maltby, C. Bygott, Photocatalytic titania based surfaces: environmental benefits, Polym. Degrad. Stab. 93 (2008) 1632–1646.
[11] M.M. Hassan, H. Dylla, L.N. Mohammad, T. Rupnow, Evaluation of the durability of titanium dioxide photocatalyst coating for concrete pavement, Constr. Build. Mater. 24 (2010) 1456–1461.
[12] S. Shen, M. Burton, B. Jobson, L. Haselbach, Pervious concrete with titanium dioxide as a photocatalyst compound for a greener urban road environment, Constr. Build. Mater. 35 (2012) 874–883.
[13] C.W.F. Yu, J.T. Kim, Photocatalytic oxidation for maintenance of indoor environmental quality, Indoor Built Environ. 22 (2013) 39–51.
[14] P. Munafò, G.B. Goffredo, E. Quagliarini, TiO2-based nanocoatings for preserving architectural stone surfaces: an overview, Constr. Build. Mat. 84 (2015) 201–218.
[15] F. Wang, L. Yang, H. Wang, H. Yu, Facile preparation of photocatalytic exposed aggregate concrete with highly efficient and stable catalytic performance, Chem. Eng. J. 264 (2015) 577–586.
[16] X. Wei, Z. Yang, S.L. Tay, W. Gao, Photocatalytic TiO2 nanoparticles enhanced polymer antimicrobial coating, Appl. Surf. Sci. 290 (2014) 274–279.
[17] J.W. Molling, J.W. Seezink, B.E.J. Teunissen, I. Muijrers-Chen, P.A.J. Borm, Comparative performance of a panel of commercially available antimicrobial nanocoatings in Europe, Nanotechnol. Sci. Appl. 7 (2014) 97–104.
[18] J.R. Pulliam, Lower infection rates after introduction of a photocatalytic surface coating, Am. J. Infect. Control 43 (2015) 180–181.
[19] Q.L. Yu, H.J.H. Brouwers, Indoor air purification using heterogeneous photocatalytic oxidation. part I: experimental study, Appl. Catal. B 92 (2009) 454–461.
[20] A. Costa, G.L. Chiarello, E. Selli, M. Guarino, Effects of TiO2 based photocatalytic paint on concentrations and emissions of pollutants and on animal performance in a swine weaning unit, J. Environ. Manage. 96 (2012) 86–90.
[21] S. Lorencik, Q.L. Yua, H.J.H. Brouwers, Design and performance evaluation of the functional coating for air purification under indoor conditions, Appl. Catal. B 168-169 (2015) 77–86.
[22] M.M. Ballari, H.J.H. Brouwers, Full scale demonstration of air-purifying pavement, J. Hazard. Mat. 254–255 (2013) 406–414.
[23] E. Boonen, A. Beeldens, Recent photocatalytic applications for air purification in Belgium, Coating 4 (2014) 553–573.
[24] T. Vasilache, I. Lazar, M. Stamate, V. Nedeff, G. Lazar, Possible environmental risks of photocatalysis used for water and air depollution case of phosgene generation, APCBEE Procedia 5 (2013) 181–185.
[25] S. Losert, N. Von Goetz, C. Bekker, W. Fransman, S.W.P. Wijnhoven, C. Delmaar, K. Hungerbuhler, A. Ulrich, Human exposure to conventional and nanoparticle-containing sprays – a critical review, Environ. Sci. Technol. 48 (2014) 5366–5378.
[26] G.S.P. Castle, Industrial applications of electrostatics: the past present and future, J. Electrostat. 51-52 (2001) 1–7.
[27] S.E. Law, Agricultural electrostatic spray application: a review of significant research and development during the 20th century, J. Electrostat. 51-52 (2001) 25–42.
[28] A. Jaworek, Electrospray droplet sources for thin film deposition, Mater. Sci. 42 (2007) 266–297.
[29] A. Jaworek, Micro- and nanoparticle production by electrospraying, Powder Technol. 176 (2007) 18–35.
[30] A. Jaworek, A.T. Sobczyk, Electrospraying route to nanotechnology: an overview, J. Electrostat. 66 (2008) 197–219.
[31] Y.-M. Tan, M.R. Flynn, Methods for estimating the transfer efficiency of a compressed air spray gun, Appl. Occup. Environ. Hyg. 17 (2002) 39–46.
[32] A. Jaworek, K. Adamiak, W. Balanchandran, A. Krupa, P. Castle, W. MacHowski, Numerical simulation of scavenging of small particles by charged droplets, Aerosol. Sci. Technol. 36 (2002) 913–924.
[33] EN 779:2012. Particulate air filters for general ventilation –Determination of the filtration performance. 2012; Classification Index: X44-012.
[34] Y.S. Cheng, Condensation detection and diffusion size separation techniques, in: P.A. Baron, K. Willeke (Eds.), Aerosol Measurements: Principles, Techniques and Applications, Wiley-Interscience, New York, 2001, pp. 569–601.
[35] A.J. Koivisto, J.E. Palomäki, A.-K. Viitanen, K.M. Siivola, I.K. Koponen, Y. Mingzhou, T. Kanerva, H. Norppa, H.T. Alenius, T. Hussein, K.M. Savolainen, K. Hämeri, Range-finding risk assessment of inhalation exposure to nanodiamonds in a laboratory environment, Int. J. Environ. Res. Public. Health 11 (2014) 5382–5402.
[36] T. Hussein, M. Kulmala, Indoor aerosol modeling: basic principles and practical applications, Water Air Soil Poll. 8 (2008) 23–34.
[37] T. Hussein, J. Smolik, V.-M. Kerminen, M. Kulmala, Modeling dry deposition of aerosol particles onto rough surfaces, Aerosol. Sci. Tech. 46 (2012) 44–59.
[38] M. Yu, A.J. Koivisto, K. Hämeri, M. Seipenbusch, Size dependence of the ratio of aerosol coagulation to deposition rates for indoor aerosols, Aerosol. Sci. Tech. 47 (2012) 427–434.
[39] Y.-M. Tan, M. Flynn, T.S.A. Buller, Field evaluation of the impact of transfer efficiency on worker exposure during spray painting, Ann. Occup. Hyg. 46 (2002) 103–112.
[40] W.C. Hinds, in: W.C. Hinds (Ed.), Aerosol Technology: Properties, Behavior, and Measurement of Airborne Particles, 2nd edn., John Wiley & Sons Inc, New York, NY, USA, 1999, pp. 233–259 (ch. 11).
[41] A.J. Koivisto, A.C.Ø. Jensen, K.I. Kling, A. Nørgaard, A. Brinch, F. Christensen, K. Jensen, Quantitative material releases from products and articles containing manufactured nanomaterials: towards a release library, Nanoimpact (2017), http://dx.doi.org/10.1016/j.impact.2017.02.001.
[42] P. Hewett, G.H. Ganser, Models for nearly every occasion: part I – one box models, J. Occup. Environ. Hyg. 14 (2017) 49–57.
[43] G.H. Ganser, P. Hewett, Models for nearly every occasion: part II – two box models, J. Occup. Environ. Hyg. 14 (2017) 58–71.
[44] ECHA, Guidance on Information Requirements and Chemical Safety Assessment, 2016, Chapter R.15: Consumer exposure estimation, available at: https://echa.europa.eu/documents/10162/13632/information_requirements_r15_en.pdf (Accessed 07 March 17).
[45] M.A. Jayjock, T. Armstrong, M. Taylor, The daubert standard as applied to exposure assessment modeling using the two-zone (NF/FF) model estimation

of indoor air breathing zone concentration as an example, J. Occup. Environ. Hyg. 8 (2011) D114–122.
[46] J.W. Cherrie, The effect of room size and general ventilation on the relationship between near and far-field concentrations, Appl. Occup. Environ. Hyg. 14 (1999) 539–546.
[47] W. Fransman, M. Van Tongeren, J.W. Cherrie, M. Tischer, T. Schneider, J. Schinkel, H. Kromhout, N. Warren, H. Goede, E. Tielemans, Advanced reach tool (ART): development of the mechanistic model, Ann. Occup. Hyg. 55 (2011) 957–979.
[48] A.J. Koivisto, A.C.Ø. Jensen, M. Levin, K.I. Kling, M. Dal Maso, S.H. Nielsen, K.A. Jensen, I.K. Koponen, Testing a near field/far field model performance for prediction of particulate matter emissions in a paint factory, Environ. Sci. Process. Impacts 17 (2015) 62.